J|A|C|S
ARTICLES
Published on Web 12/15/2006

Composite Particles of Polyethylene @ Silica

Hanan Sertchook,[†] Hila Elimelech,[†] Carina Makarov,[‡] Rafail Khalfin,[‡] Yachin Cohen,[‡] Michael Shuster,[§] Florence Babonneau,[||] and David Avnir*,[†]

Contribution from the Institute of Chemistry, The Hebrew University of Jerusalem, Jerusalem 91904, Israel, Faculty of Chemical Engineering, Technion-Israel Institute of Technology, Haifa 32000, Israel, Carmel Olefins Ltd., P.O.B. 1468, Haifa 31014, Israel, and Chimie de la Matiere Condensee, Universite Paris 6 - T54-E5, 4 Place Jussieu, 75252 Paris Cedex 05, France

Received July 25, 2006; E-mail: david@chem.ch.huji.ac.il

Abstract: Polyethylene (PE) and silica are perhaps the simplest and most common organic and inorganic polymers, respectively. We describe, for the first time, a physically interpenetrating nanocomposite between these two elementary polymers. While polymer−silica composites are well known, the nanometric physical blending of PE and silica has remained a challenge. A method for the preparation of such materials, which is based on the entrapment of dissolved PE in a polymerizing tetraethoxysilane (TEOS) system, has been developed. Specifically, the preparation of submicron particles of low-density PE@silica and high-density PE@silica is detailed, which is based on carrying out a silica sol−gel polycondensation process within emulsion droplets of TEOS dissolved PE, at elevated temperatures. The key to the successful preparation of this new composite has been the identification of a surfactant, PE-b-PEG, that is capable of stabilizing the emulsion and promoting the dissolution of the PE. A mechanism for the formation of the particles as well as their inner structure are proposed, based on a large battery of analyses, including transmission electron microscopy (TEM) and scanning electron microscopies (SEM), surface area and porosity analyses, various thermal analyses including thermal gravimetric analysis (TGA/DTA) and differential scanning calorimetry (DSC) measurements, small-angle X-ray scattering (SAXS) measurements and solid-state NMR spectroscopy.

Introduction

Surprising as it may sound, physically interpenetrating polymeric composites made of the most common inorganic polymer, silica (SiO_2), and of the most common organic polymer, polyethylene (PE), to the best of our knowledge, are not known. The ruling ways to blend these different polymers have been either to disperse silica powders as fillers within PE, which is by now a well-developed technology with many applications[1] or to polymerize ethylene within the pores of modified[2] or unmodified silica.[3] The preparation of interpenetrating polymers[4] and of silica-polymer composites[5] are well-known, and yet the intimate blending of silica and PE remained a challenge because of the very different nature of these polymers and because of the general difficulty in handling PE, which is devoid of any functional group. Here, we describe a general method for the preparation of PE@silica interpenetrating composites and demonstrate it for both low-density and high-density PE (LDPE and HDPE, respectively) in the form of submicron particles. The method with which this goal has been achieved is based on dissolving linear PE in a boiling solution of tetraethoxysilane (TEOS) in xylene and emulsifying this hot solution in an alkaline hydrophilic (water−alcoholic) dispersing solution. The base then catalyzes the polycondensation of the TEOS to silica within the emulsion droplets, entrapping the PE while the silica network forms. It is a novel approach in the sense that the standard method for preparing composites of organic polymers with inorganic oxides has been to polymerize the former in the presence of the latter and we are reversing it: the ready organic polymer is entrapped in a forming oxide

[†] The Hebrew University of Jerusalem.
[‡] Technion-Israel Institute of Technology.
[§] Carmel Olefins Ltd.
[||] Universite Paris 6 - T54-E5.

(1) (a) Reddy, C. S.; Das, C. K. *Polym. & Polym. Compos.* **2006**, *14*, 281−290. (b) Ouyang, C.; Wang, S. F.; Zhang, Y.; Zhang, Y. X. *J. Appl. Polym. Sci.* **2006**, *101*, 472−479. (c) Huang, Y.; Jiang, S.; Wu, L.; Hua, Y. *Polym. Test* **2004**, *23*, 9−15. (d) Van Dyke, J. D.; Gnatowski, M.; Burczyk, A. *J. Appl. Poly. Sci.* **2002**, *83*. 2562−2578. (e) Sumita, M.; Tsukihi, H.; Miyasaka, K.; Ishikawa, K. *J. Appl. Polym. Sci.* **1984**, *29*, 1523−1530. (f) Howard, E. G.; Lipscomb, R. D.; MacDonald, R. N.; Glazar, B. L.; Tullock, C. W.; Sumita, M.; Ookuma, T.; Miyasaka, K. *J. Appl. Polym. Sci.* **1982**, *27*, 3059−3066. (g) Collete, J. W. *Ind. Eng. Chem. Prod. Res. Dev.* **1981**, *20*, 421. (h) Howard, E. G.; Glazar, B. L.; Collete, J. W. *Ind. Eng. Chem. Prod. Res. Dev.* **1981**, *20*, 429.
(2) Monteil, V.; Stumbaum, J.; Thomann, R.; Mecking, S. *Macromolecules* **2006**, *39*, 2056−2062.
(3) (a) Tajima, K.; Ogawa, G.; Aida, T. *J. Polym. Sci., Part A: Polym. Chem.* **2000**, *38*, 4821−4825. (b) Kageyama, K.; Tamazawa, J.; Aida, T. *Science*, 1999, *285*, 2113−2115.
(4) (a) Kusuktham, B. *J. Appl. Polym. Sci.* **2006**, *102*, 1585−1591. (b) Tsutsui, H.; Moriyama, M.; Nakayama, D.; Ishii, R.; Akashi, R. *Macromolecules* **2006**, *39*, 2291−2297. (c) Saendee, P.; Tangboriboonrat, P.; *Colloid Polym. Sci.* **2006**, *284*, 634−643.
(5) (a) Yilmaz, E.; Ramstrom, O.; Moller, P.; Sanchez, D.; Mosbach, K. *J. Mater. Chem.* **2002**, *12*, 1577−1581. (b) Choi, M.; Kleitz, F.; Liu, D.; Lee, H. Y.; Ahn, W. S.; Ryoo, R. *J. Am. Chem. Soc.* **2005**, *127*, 1924−1932. (c) Chen, W. Y.; Ho, K. S.; Hsich, T-H.; Chang, F-C.; Wang, Y-Z. *Macromol. Rapid Commun.* **2006**, *27*, 452−457.
(6) (a) Sertchook, H.; Elimelech, H.; Avnir, D. *Chem. Mater.* **2005**, *17*, 4711 − 4716. (b) Mokari, T.; Sertchook, H.; Aharoni, A.; Ebenstein, Y.; Avnir, D.; Banin, U. *Chem. Mater.* **2005**, *17*, 258−263.

 10.1021/ja0653167 CCC: $37.00

Table 1. The Polyethylene@Silica Samples Studied in This Report

sample	type of PE and amount (g)[a]	amount of PE-b-PEG, g	alcohol in the hydrophilic phase	PE/PE-b-PEG ratio (w-PE/w-surfactant)	particles average size, nm (standard deviation, %)
1	LDPE (0.07)	0.3	2-propanol	1:4	285 (15)
2	LDPE (0.07)	0.3	ethanol	1:4	153 (15)
3	LDPE (0.17)	0.27	2-propanol	1:1.5	
4	LDPE (0.2)	0.2	ethanol	1:1	
5	LDPE (0.2)	0.1	ethanol	2:1	191 (24)
6	LDPE (0.2)	0.067	ethanol	3:1	161 (16)
7	LDPE (0.2)	0.05	ethanol	4:1	104 (18)
8	LDPE (0.2)	0.04	ethanol	5:1	225 (41)
9	LDPE (0.2)	0.033	ethanol	6:1	290 (17)
10	LDPE (0.2)	0.028	ethanol	7:1	240 (19)
11	HDPE (0.04)	0.3	ethanol	1:7.5	153 (15)
12	HDPE (0.12)	0.3	ethanol	1:2.5	249 (17)
13	none	0.4	ethanol	surfactant only	147 (15)

[a] 2.0 mL of TEOS in all compositions.

matrix.[6] The identification of the suitable surfactant and the formation of a stable emulsion are the crucial steps. For the formation of the PE@SiO_2 composite, the surfactant of choice was found to be polyethylene-*block*-poly(ethyleneglycol) (PE-b-PEG, Mw 1400 g/mol), and the rational for its successful operation is explained below. We first describe how to prepare the novel PE@silica particles and then present and discuss some of their properties and the proposed mechanism of their formation.

2. Experimental Details

2.1. Preparation of the PE@SiO2 Particles. Preparation of LDPE@SiO_2 Particles. In a typical procedure (sample 7, Table 1), 0.2 g of LDPE (density of 0.932 g/mL, melting index of 55 gr/min, Aldrich) and 0.05 g of the surfactant PE-b-PEG (Mw 1400, PE/PEG = 1:1 by weight, Aldrich) were placed in a vial and were heated until melting, then 4.0 mL of boiling xylenes was added (137−144 °C) until there was a full dissolution of the melt (at least 20 min). To this hot solution, 2.0 mL of TEOS (Aldrich) was added and mixing continued until a clear solution was obtained. The dispersing hydrophilic phase was prepared by mixing 50 mL of ethanol (or 2-propanol, see Table 1) with 30 mL of ammonium hydroxide solution (25% by weight NH_3) followed by heating the solution to the boiling point. To this hot solution, the boiling hydrophobic phase was added quickly dropwise and under vigorous stirring, and the mixture brought close to its boiling point (∼78 °C). After the addition, a stable emulsion formed immediately that was allowed to boil for about 30 min, and then the emulsion/dispersion was allowed to cool slowly under mild stirring (magnetic stirrer) for 18−24 h while the particles continued to form. For collecting and cleaning the particles, the resulting dispersion was centrifuged at 6000 rpm for 20 min and the precipitate redispersed in either water or ethanol. For characterization purposes, the powder was dried at 100 °C for several hours. From thermal gravimetric analysis (TGA) (see below), the composition of the final particles is typically 1:∼2 by weight. Other surfactants, listed in Results and Discussion, were tested by similar procedures either with tetramethoxysilane (TMOS) or with TEOS, but none lead to satisfactory results. For blank tests, the surfactant was entrapped within silica without PE using the same procedure. Table 1 contains other tested compositions that led to the particles formation.

Preparation of HDPE/SiO_2 Particles. In a typical procedure (sample 12, Table 1), the hydrophobic phase was prepared by heating 0.12 g of HDPE (density of 0.950 g/mL and Mw of 125 000; Aldrich) and 0.3 g of PE-b-PEG until the mixture melted (∼130 °C). To this melt, 4.0 mL of boiling xylenes (137−144 °C) was added and the mixture was stirred until total dissolution, a process that took up to 2 h. Refluxing for 2 h is crucial, even if visually the solution is homogeneous at a shorter time. Then, 2.0 mL TEOS was added and mixing continued under heating until a clear solution was obtained. From this point on, the procedure is as for LDPE.

2.2. Instrumentation and Measurement Conditions. Microscopy. Transmission electron microscopy (TEM) was performed with a Philips CM12 instrument from the Technai Series, operated at 100 kV. Samples were prepared by depositing an ethanolic or aqueous solution of the particles on a Formvar/Carbon 300 mesh copper grid. High-resolution scanning electron microscopy (HR-SEM) was performed with a Sirion (FEI) microscope, operating at 5 or 10 kV. Samples were prepared by placing the centrifuged, air-dried powder on an aluminum stub using a double-sided tape.

Particle Size Analysis. The diameters of at least 200 particles were determined for each sample using Analysis software, and the statistical analysis was carried out with KaleidaGraph (from Synergy Software). The particle sizes for most of the samples are collected in Table 1.

TGA/DSC. TGA were carried out with an SDT 2960 V3.0F (TA Instruments) under air at rate of 10 °C/min. *DSC*: Differential scanning calorimetry (DSC) measurements were carried out with a Perkin-Elmer DSC-7 instrument, using Pyris software. The measurement procedure, under nitrogen atmosphere, included the following steps: (1) Equilibrating the sample for 1 min at 60 °C; (2) heating from 60 to 180 °C at a rate of 10 °C/min; (3) holding for 3 min at 180 °C; (4) cooling from 180 to 60 °C at a rate of 10 °C/min; (5) holding for 1 min at 60 °C; and (6) heating from 60 to 180 °C at a rate of 10 °C/min.

Surface Area and Porosity Analysis. Nitrogen Brunauer−Emmett−Teller (BET) surface area and porosity were determined from adsorption/desorption isotherms on a Micromeritics ASAP-2000 physisorption instrument, using the BET and the Barrett−Joyner−Halenda (BJH) equations, respectively.

SAXS. Small-angle X-ray scattering (SAXS) measurements were performed using a slit-collimated compact Kratky camera with Cu Kα radiation (sealed tube generator operated at 30−40 kV and 15−25 mA and Ni filtered), slit height 20 μm and length 15 mm. The scattering intensity was recorded using a linear position-sensitive detector (Raytech) in the interval $0.08 < h < 3.0$ nm^{-1}, where h is the scattering vector defined as

$$h = (4\pi/\lambda)\sin(\theta), \qquad (1)$$

where 2θ is the scattering angle and λ is the wavelength (0.1542 nm). The sample temperature was retained at 22 °C. The particles' dispersions in water were sealed in thin-walled glass capillaries of about 2 mm diameter and 0.01 mm wall thickness. The scattered SAXS intensity, $I_s(h)$, was normalized to the following parameters: time, solid angle, primary beam intensity, capillary diameter, transmission, and the Thompson factor. The scattering from the solvent and empty capillary was subtracted. The SAXS intensity measured using a slit-collimated

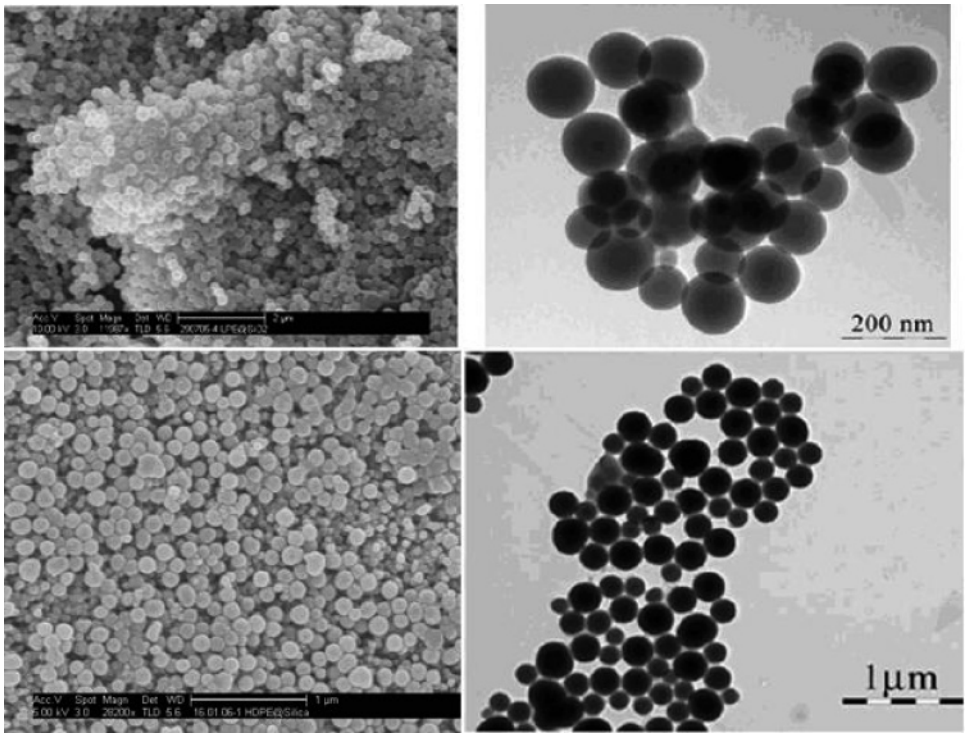

Figure 1. SEM (left) and TEM (right) of LDPE@silica (top, sample 7) and of HDPE@silica (bottom, sample 12). (Bars: 200 nm and 2 μm for the TEM and SEM of LDPE@silica, respectively; 1 μm for the SEM and TEM of HDPE@silica.)

incident beam is termed "smeared intensity". Correction for the smearing effect of the incident beam dimensions and data reduction were performed with Glatter's indirect Fourier transformation procedure (ITP),[7] to yield the "desmeared intensity" $I_d(h)$, and the distance distribution function $P(r)$, defined below.

Solid-State NMR. NMR measurements were performed on a Bruker AVANCE 300 spectrometer at $B_0 = 7$ T with $\nu_0(^1H) = 300.13$ MHz, $\nu_0(^{13}C) = 75.47$ MHz and $\nu_0(^{29}Si) = 59.63$ MHz, using a 4 mm triple resonance Bruker MAS probe. Samples were spun at the magic angle using ZrO_2 rotors (10 kHz). ^{29}Si and ^{13}C magic-angle spinning (MAS) NMR spectra were recorded with high-power $\{^1H\}$ decoupling ($\approx$ 50 kHz) during acquisition, using 90° pulse and 100-s recycle delays. ^1H spectra were obtained with 90° pulse duration and 3-s recycle delays. For cross-polarization (CP) experiments under MAS, the radio frequency field strength for ^1H was ca. 50 kHz. ^1H and ^{29}Si chemical shifts were referenced to tetramethylsilane (TMS).

3. Results and Discussion

3.1 Obtaining the Particles. Some typical SEM and TEM pictures of the composite particles are collected in Figure 1. It can be seen that they are well defined and spherical, between 150 and 290 nm in size (Table 1). The two main experimental difficulties in obtaining the successful emulsion for the preparation of the composite particles within the droplets of a water/oil (W/O) emulsion have been the low solubility of semicrystalline PE, and the identification of a suitable surfactant for stabilizing the emulsion (at least) for the duration of the time needed to begin the formation of the silica network. The low solubility of PE required the use of elevated temperatures; thus, the oil phase in the O/W emulsion was a hot xylenes/TEOS solution of PE, and the dispersing phase was a hot alcohol−water solution of ammonia (which resembles the classical solvent for Stöber-type processes[8]). As for the surfactant, a wide variety has been tested, including the anionic surfactants sodium dodecylsulfate (SDS) and aerosol OT (AOT), the cationic cetyltrimethylammonium bromide (CTAB) and p-toluenesulfonate, and the non-ionic Triton X-100, Span 80, Tween 20 and DOW 190, and PE-b-PEG. Of these, only CTAB and PE-b-PEG formed a stable emulsion.[9] PE-b-PEG is a block copolymer (MW ~1400 g/mol) surfactant in which the weight ratio of the two blocks is 1:1 and it provides an HLB ratio of 10, making it suitable for the formation of O/W emulsions. The success of this surfactant is attributed to the good compatibility of the two blocks with the two phases: the PE block is of course most suitable for the PE-solution phase (indeed the similarity of the behavior of the two PE chains was confirmed by differential scanning calorimetry (DSC) analysis (below)), and the PEG block is highly compatible with the water alcohol phase.

The structure of the surfactant is shown below.

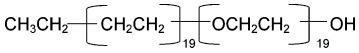

As indicated in Table 1, various surfactant/LDPE weight ratios were tested toward the formation of LDPE@silica from 4:1 (a large excess of the surfactant) to 1:7 (a large excess of the polymer). Monomodal size distributions ranging from 100 to 290 nm are obtained with the smallest particles at a surfactant/LDPE = 1:4 ratio; some typical distributions are collected, as mentioned above, in Table 1. An interesting solvent effect on particle size is seen by comparing samples 1 and 2. The particles, which were prepared in 2-propanol, are larger by about 100 nm compared to those prepared in ethanol using similar

(7) Glatter, O. *J. Appl. Crystallogr.* **1977**, *10*, 415.
(8) Stöber, W.; Fink, A.; Bohn, E. *J. Colloid Interface Sci.* **1968**, *26*, 62−69.
(9) CTAB stabilized the emulsion as a bicontinuous phase and not as discrete particles, and therefore CTAB can be used for preparation of PE@silica composite blocks and films (which are also new, but are not the topic of this report).

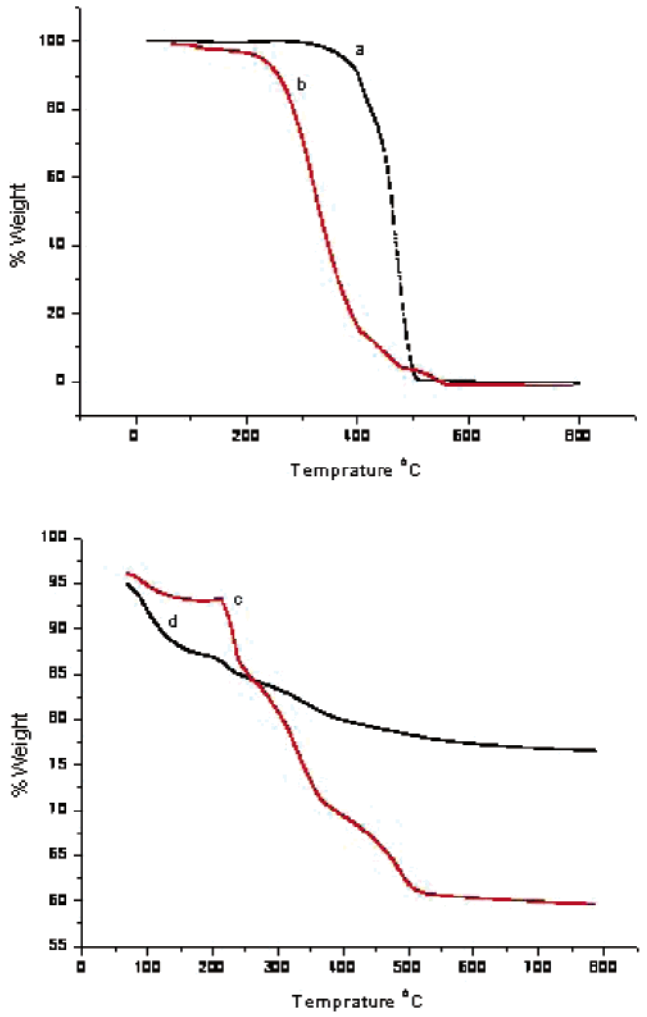

Figure 2. (Top) TGA of the free components: (a) linear low-density polyethylene; (b) the surfactant, polyethylene-*block*-polyethylene glycol. (Bottom) TGA of the entrapped components: (c) LDPE@silica (sample 7); (d) PE-b-PEG@silica (sample 13).

compositions; indeed, this is in agreement with similar observations in Stöber processes in which the increase in the alcohol alkane chain was found to cause such an effect.[8] As for the needed amount of surfactant, below a ratio of 1:4, some of the LDPE began not to be entrapped, and below a ratio of 1:7, a stable emulsion was not formed. In conclusion, for LDPE@silica, our recommendation therefore is to use a ratio of 1:3 to 1:4 in ethanol for efficient entrapment and particle formation.

As for HDPE@silica, the main difficulty was the slow dissolution rate in the xylenes + TEOS; at least 2 h of reflux and a large excess of surfactant were needed for full dissolution and formation of a stable emulsion (Table 1). For reference purposes, particles in which only the surfactant was entrapped were prepared, resulting again in well-defined particles (∼150 nm, sample 13, Table 1).

3.2. Particle Characterizations. 3.2.1. Thermal Analyses. TGA. The most elementary proof for the composite nature of the particles is its oxidative thermal weight-loss behavior, which has indicated a composition of about 60% of silica and 40% of organics. All samples showed a similar decomposition pattern of four degradation weight-loss steps, and a typical example (sample 7) is shown in Figure 2. To comment on these steps, we shall first observe the results of two blank-TGA experiments: the TGA of free, neat LDPE (Figure 2, top) shows practically a single step in the range of ∼390−500 °C. The TGA of the free, neat surfactant is more widespread, reflecting the fact that it is a block-copolymer: decomposition starts already at 200 °C (apparently of the PEG portion), continues smoothly until 400 °C, followed then by two smaller steps of one at 400 − 480 °C and the last one reaching even beyond the range of the TGA of PE, ending at 540 °C; it seems reasonable to suggest that the higher temperature range reflects mainly the PE moiety of the surfactant. As for LDPE@silica (Figure 2, bottom), the first drop in weight (up to ∼210 °C) is due to solvents loss (water, xylenes, ethanol). The next two steps, 210−250 and 250−350 °C, overlap the decomposition range of the free surfactant. Note that whereas the free surfactant has one-step decomposition, the entrapped has two; below we shall provide more evidence that the surfactant is entrapped in at least two distinct crystalline forms. Finally, the last weight-loss step, 350 − 550 °C, is due to the decomposition of the PE. The fact that separate steps are seen, although as expected, broadened, shows that the blending of the surfactant and the PE is only partial; had it been full, one would expect a smoother profile. Again additional support to that observation is provided below.

DSC. Figure 3 shows the DSC profiles of (un-entrapped) LDPE, HDPE, and PE-b-PEG. As is expected from the different nature of the two polymers, the melting and crystallization temperatures for HDPE are higher (131.4, 115.3 °C, respectively; Figure 3b) than those of the LDPE (110.7, 96.6 °C, respectively; Figure 3a), reflecting larger (thicker) lamellar domains in HDPE. The surfactant, PE-b-PEG, exhibits in the DSC analysis two overlapping endothermic peaks on heating (melting) and two overlapping exothermic peaks on cooling (crystallization) (Figure 3c). The fact that the higher temperature pair, (the endothermic peak at 103.0 °C and the exothermic peak at 96.0 °C) is close to those of the corresponding LDPE peaks allows one to associate them with the crystallinity of the surfactant's oligomeric PE block (melting of the PEG block is expected at ∼60 °C). This is also confirmed by NMR (below), which indicates high mobility of the PEG block, characteristic for a noncrystalline phase. The presence of a lower temperature pair of peaks (the broad endothermic peak on heating at 93.8 °C and the broad exothermic peak on cooling at 87.5 °C) implies the presence of a second, less ordered crystalline phase associated with the PE block. A second crystalline phase is present also in LDPE, as seen by the low-temperature shoulders adjacent to both the melting and the crystallization peaks (Figure 3a). One is led to propose that the PE block of the surfactant, similar to the LDPE, crystallizes in two forms, differing in the lamellae thickness. Note, however, that the relative content of the low-temperature crystalline form in the surfactant, is higher and that the relative weight of the two crystalline phases changes somewhat upon entrapment, reducing the high-temperature fraction and increasing the second one (Figure 4a). This trend of change is even more pronounced in the composite HDPE@silica (sample 12, Figure 4b), making the lower-temperature crystalline phase of PE-b-PEG the dominant one. By assuming that the low-temperature phase is associated with a less ordered crystalline structure, these changes reasonably indicate an increase in overall structure disorder due to the entrapment and to partial blending with the PE block of the surfactant. As for the HDPE

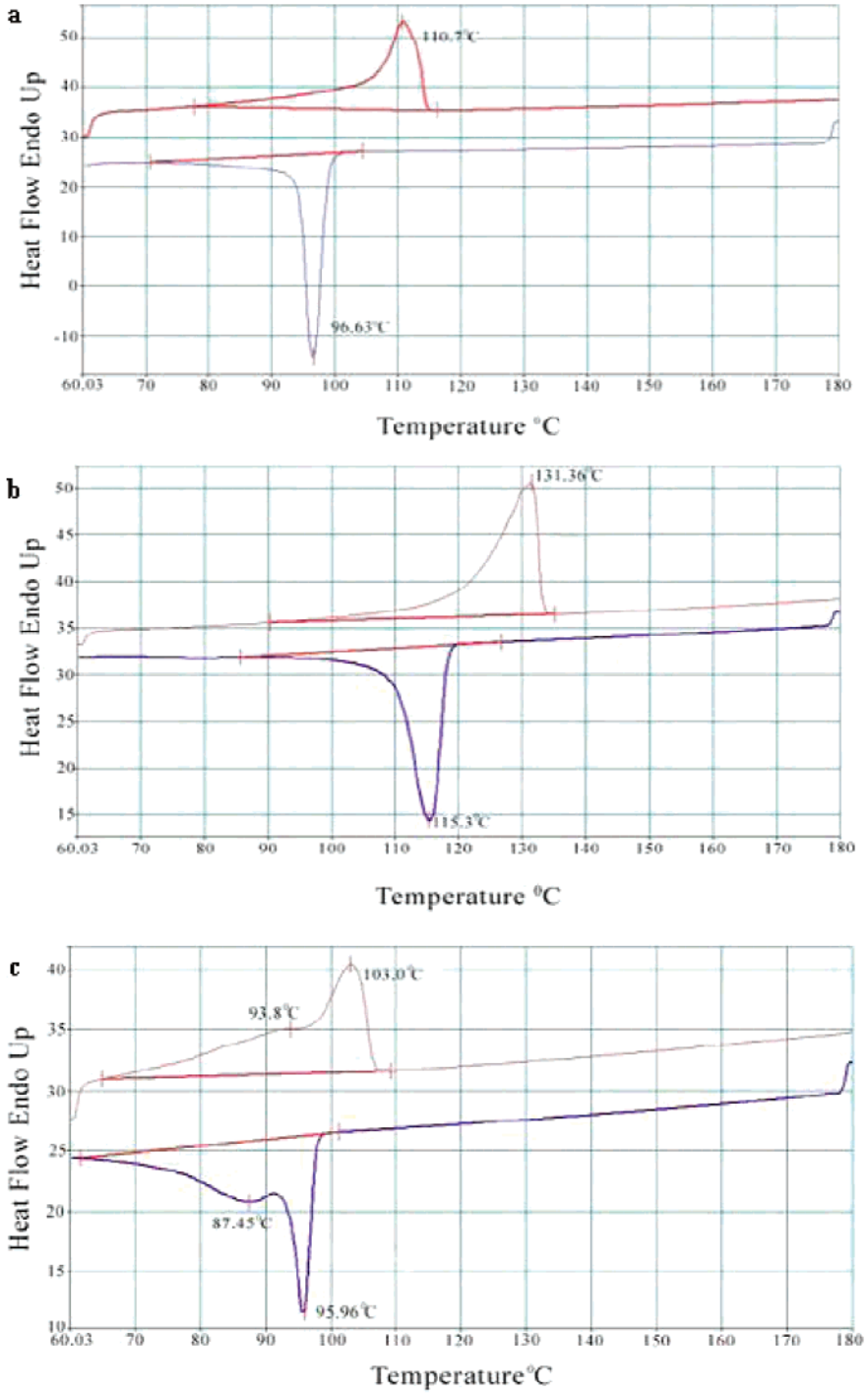

Figure 3. DSC spectra of the free individual components samples: (a) linear low-density polyethylene; (b) high-density polyethylene; (c) PE-b-PEG.

itself in HDPE@silica, there is a decrease in the melting and crystallization temperatures (Figure 4b), indicating again an overall decrease of the weight of the PE lamellar phase due to the entrapment. As for LDPE@silica, there is an overlap between the peaks of the polymer and of the surfactant (sample 4, Figure 4c), and therefore a similar detailed analysis is not possible; Figure 4c is shown for completeness of the report.

Degree of Crystallinity. DSC allows one to get an approximate evaluation of the degree of crystallinity of the entrapped HDPE (but not of the entrapped LPDE because of the overlap with the surfactant). For the free HDPE, the degree of crystallinity is ~60% (59.6%, based on the melting heat value of 174.7 J/g and the usually assumed specific melting heat value of 293.6 J/g for extrapolated 100% crystalline PE[10]). As for HDPE@silica, from the melting heat of the HDPE component, 8.8 J/g, and the weight fraction of about 10% (from TGA), one can estimate a crystallinity of ~30%. This lower value for the entrapped HDPE compared to the free one makes sense: the entrapped HDPE lost part of its crystallinity both by the dissolution in the surfactant phase and by the restriction to crystallize, imposed by the interwoven silica phase; in fact, it

(10) Wunderlich, B. *Thermal Analysis*; Academic Press: New York, 1990; p. 418.

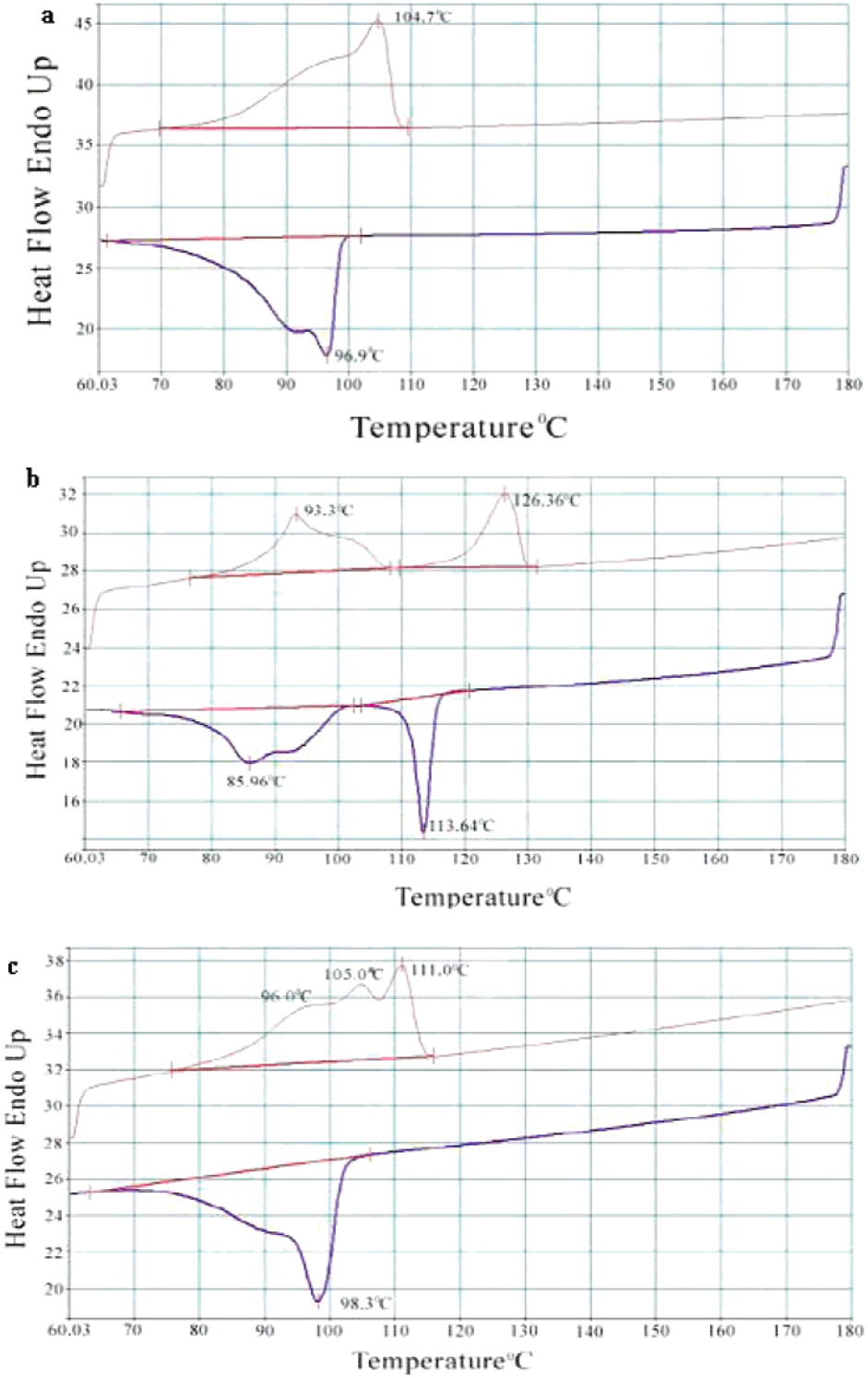

Figure 4. DSC spectra of the composite samples: (a) PE-b-PEG@silica (sample 13); (b) HDPE@silica (sample 12); (c) LDPE@silica (sample 4).

is interesting that some of the HDPE still retains the crystal form. In the size-domain distribution of the PE, the crystalline phase increases as one goes from the left (small domains) to the right tail in that distribution.

3.2.2. Nondestructive Analyses. Surface Area and Porosity. These measurements indicate that the polymer occupies the voids of the silica substructure; namely, they are quite nonporous. Thus, the surface areas are small, typically 7.9 m^2/gr (sample 7), with residual macroporosity of 0.080 mL/gr and with the average pore size of 28 nm; the last two values may be due to only interstitial porosity.

SAXS. SAXS proved to be a useful tool in many studies of composite, multiphase materials,[11] because the inner structure provides the needed contrast variations at the interfaces between the phases. Moreover, in our measurements the particles were suspended in water, providing an additional contrasting interface,

(11) Glatter, O. *J. Appl. Crystallogr.* **1980**, *13*, 7.

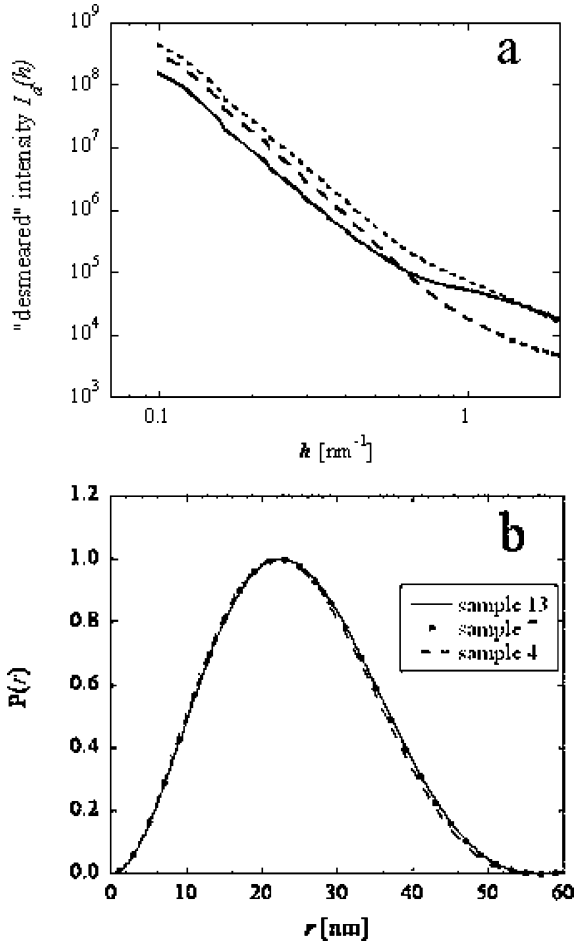

Figure 5. Typical SAXS observations: (a) the desmeared scattering patterns, and (b) the distance distribution functions, $P(r)$ of solid line, sample 13; dashed line, sample 7; dotted line, sample 4.

namely that of the whole particle. However, because the particle size is larger than the dimensions that can contribute to significant scattering in the measured angular range, we interpret the scattering patterns as predominantly due to the inner structure. The characteristics of the inner particle structure can be obtained from the SAXS measurements by evaluating its distance distribution function, $P(r)$, which is the Fourier transformation of the desmeared SAXS intensity $I_d(h)$:[7]

$$P(r) = \frac{r^2}{2\pi^2}\int_0^\infty I(h)\frac{\sin(hr)}{hr}h^2 dh \qquad (2)$$

The $P(r)$ function was used to evaluate correlation distances within the inhomogeneous particles. The desmeared scattering patterns from samples 4, 7, and 13 do not deviate significantly from each other, as shown in Figure 5a, indicating an inner structure that is not sensitive to the specific composition. Porod's law, $I_d(h) \sim h^{-4}$, is obeyed in the range of $0.2 < h < 0.8$, which indicates a smooth interface in the inner structure. The curves for the distance distribution function $P(r)$, are identical (Figure 5b) and rather symmetric with a maximum at about 22 nm. This value is a radius of correlation of that distance for the inner pore structure. The fact that this structural feature is unaffected by the polymer loading shows that the sol−gel process forming the silica matrix remains undisturbed by the polymer solution, a conclusion corroborated also by the solid-state NMR results (below). A detailed SAXS analysis of these novel materials using the contrast variation technique will be reported separately.

NMR. An interesting observation was made by employing ^{29}Si MAS NMR spectrum analysis of the PE@silica particles (sample 7, Figure 6a): when deconvoluted, three signals at −95.1, −101.8, and −111.2 ppm assigned to the Q^2, Q^3, and Q^4 units (bi-, tri-, and tetrabranching, respectively) appear. The relative intensities, 5:29:66 indicate a degree of condensation of ∼90%, which corresponds to a highly condensed silica network. Thus, we reach again the conclusion, obtained from the SAXS measurements, that within the emulsion droplet the sol−gel polycondensation takes place without disturbance from the polymer.

The $^{13}C\{^1H\}$ NMR spectrum of the composite particles (Figure 6b) shows three main peaks at 30.7 and 33.0 ppm due to the PE blocks and at 71.3 ppm due to the PEG blocks. Integration gives a PEG/PE molar ratio around 10%. CP experiments show a different behavior of the two PE components that can be assigned to noncrystalline (30.7 ppm) and crystalline (33.0 ppm) components. The difference in mobility between the two components can be shown by a $^1H \rightarrow {}^{13}C$ heteronuclear correlation (HETCOR) two-dimensional (2D) spectrum (not shown) recorded at a moderate MAS rate (10 kHz), which prevents averaging of strong homonuclear $^1H-{}^1H$ dipolar coupling. Consequently, ^1H resolved resonance peaks are only expected for protons in mobile parts, while signals corresponding to protons in rigid segments will be very broad. Indeed, the ^{13}C resonance peak at 30.7 ppm (mobile noncrystalline PE-component) corresponding to a sharp ^1H peak at 1.4 ppm, while the peak at 33 ppm (rigid crystalline PE-component) is related to a very broad ^1H signal that extends over 10 kHz. For the composite particles, simulation of the peak intensities due to the PE components gives a noncrystalline-to-crystalline ratio of 56:44 that is comparable to what was found is the starting linear PE (55:45).

The ^1H MAS NMR spectrum recorded at similar MAS rate (10 kHz) (Figure 6c) shows three resolved peaks at 1.4, 3.7, and 5.8 ppm, assigned to the CH_2 protons in the mobile, noncrystalline PE, to the CH_2 protons in PEG, and to OH groups, respectively. From the $^1H-{}^{13}C$ HETCOR experiment (not shown), the ^1H signal due to the crystalline PE component is very broad and certainly related to the spinning side bands that can be observed over a rather large frequency range in the ^1H MAS NMR spectrum.

Once the various ^1H resonance peaks have been assigned, the ^1H and ^{29}Si one-dimensional (1D) spectra can be correlated through the $^1H \rightarrow {}^{29}Si$ HETCOR 2D spectrum (Figure 7), to provide information on the interaction between the two phases, the silica network, and the organic components (PE and PE-b-PEG). No correlation peak is visible over a large ^1H chemical shift range, indicating that the silica network is not in close proximity with the rigid crystalline PE segments. The main cross peaks involve the Q^3 sites that are primarily interacting with OH protons ($\delta = 6$ ppm) and to a lower extent with the $O-CH_2$ groups of the PEG segments ($\delta = 4$ ppm) (Figure 7). The cross peaks involving Q^4 sites are of low intensity and do not show any preferential interactions with the various protons. Thus, this

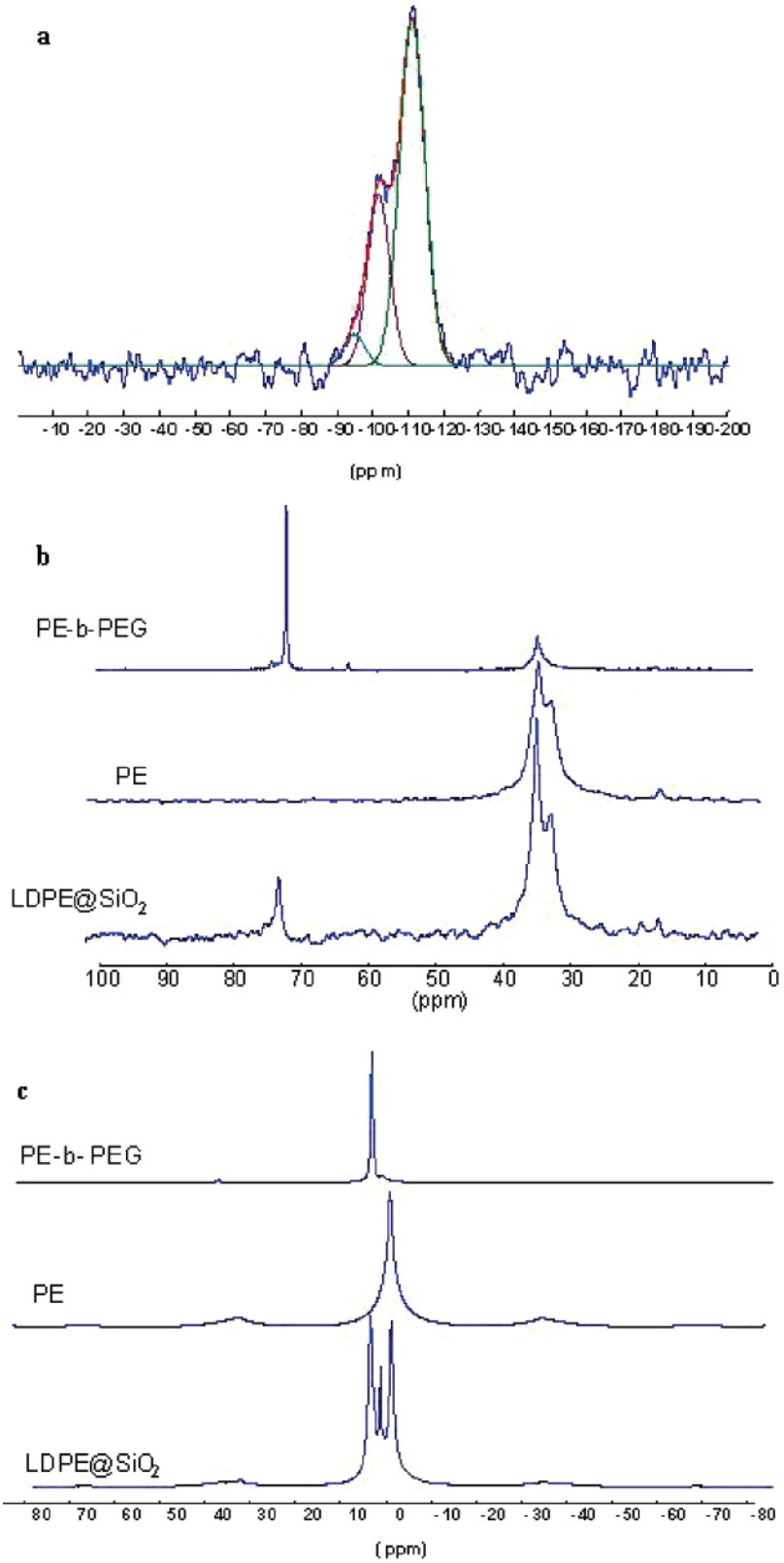

Figure 6. NMR spectra of LDPE@silica (sample 7). (a) The ^{29}Si MAS NMR spectrum. (b) The ^{1}H{^{13}C} NMR spectrum. (c) The ^{1}H MAS NMR spectrum of the composite (bottom); the NMR spectra of the organic components are shown as well.

spectrum seems to indicate that the surfactant mediates between the PE and the silica network, namely, its PEG portion points to the silanols of the silica pore network, while the PE merges into the LDPE phase.

4. The Overall Picture and Conclusions

Detailed analysis of the various experimental observations was provided above, but we find it useful to provide now an overall picture that is based on all the observations and

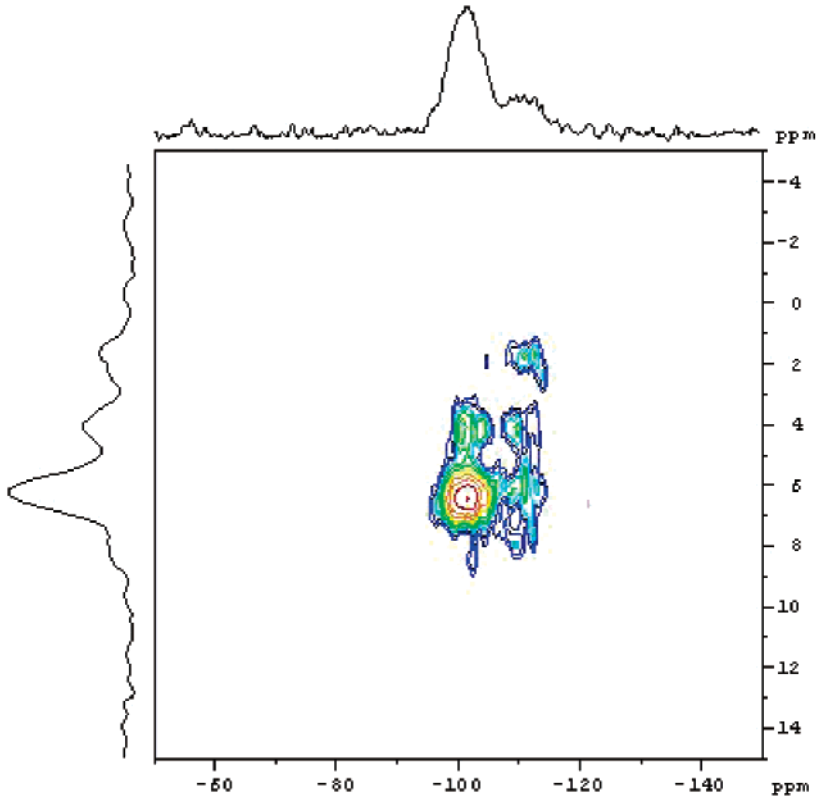

Figure 7. The $^{1}H \rightarrow {}^{29}Si$ HETCOR 2D spectrum of LDPE@silica (sample 7). Vertical axis: ^{1}H. Horizonal axis: ^{29}Si.

measurements presented above. The following picture is proposed for the mechanism of the particles formation and for their inner structure (Scheme 1). The first stage is the drop formation step. Here it is clear that the surfactant plays a role not only in the stabilization of the forming emulsion, but that it actively facilitates the dissolution process of the polymer, which cannot be carried out without its presence: The "like-dissolves-like" principle operates here with the PE portion of the PE-b-PEG. Stabilization of the oily droplet is due to the two portions of the surfactant, each of which is very compatible with one of the two phases: PEG with the water/ethanol phase, and PE with the TEOS/xylene/PE phase (in which it is likely that the PE chains are fairly stretched). The second stage is the formation of a silica thin blanket on the surface of the droplet. The silica formation begins at the droplet interface in which the base meets TEOS. Interestingly, the final composite is not of a core-shell architecture, and the third stage is the composite particle formation of interpenetrating domains of PE and silica. Phase separation that does occur, as evident from the existence of crystallinity in the composite (DSC), is limited to domains of the order of 20 nm (SAXS), the size of which is primarily dictated by the polycondensed TEOS. To understand why the final particle resembles more an interpenetrating network of an organic and an inorganic polymer, we propose that the formation of the initial silica at the interface, creates a diffuse zone with both hydrophilic (SiOH) and hydrophobic (SiOEt) residues that facilitate the mixing of the aqueous base with the (partially hydrolyzed, oligomerized) TEOS; in a sense, this forming silica zone acts as the "cosolvent" which is routinely used in sol−gel procedures. As the silica network continues to form, it becomes more and more difficult for the PE to separate, because it is more interpenetrated with the porous inorganic matrix. At the end of this process, as is clearly evident from the DSC and NMR analyse, the PE and the PE-b-PEG are distributed among several packaging forms: there are domains of crystalline phases (DSC), of separated PE and PE-b-PEG amorphous domains (NMR), and of domains in which the PE and PE-b-PEG are blended. Also interesting is that the organic polymer does not interfere with the silica structure. We attribute this to the fact the TEOS polycondensation is a three-dimensional (3D) highly cross-linking process, while the linear PE has the flexibility to adapt to the silicate structure.

In preparing particles of PE@silica, we have extended the general approach of forming organic/inorganic composite particles by entrapping the desired polymer from viscous polymers (polystyrene@silica and PDMS@silica[6]) to semicrystalline polymers. It should be noted that the PE-b-PEG@silica particles, the preparation of which was also described here, add to the list of various types of polymer@silica particles block copolymers as well. As we have already shown for the preparation of polystyrene@silica particles[6b,12] and PDMS@silica composite particles,[6a] identification of the suitable surfactant and the formation of a stable emulsion are the crucial steps. Further studies of various polyethylenes@silica, as well as of other types of polymers, are in progress to explore in full the scope of the methodology of composite particle formation by entrapment within a forming sol−gel particle and to explore possible applications. Preliminary studies point to an important application of the PE@silica particles, namely the ability to disperse them homogeneously in polyolefins due to the PE chains on the surface of the particles (based, again, on "like-

(12) Sertchook, H.; Avnir, D. *Chem. Mater.* **2003**, *15*, 1690−1694.

Scheme 1. The Three Stages of the Mechanism of Formation of the Particles. See Text for Explanation

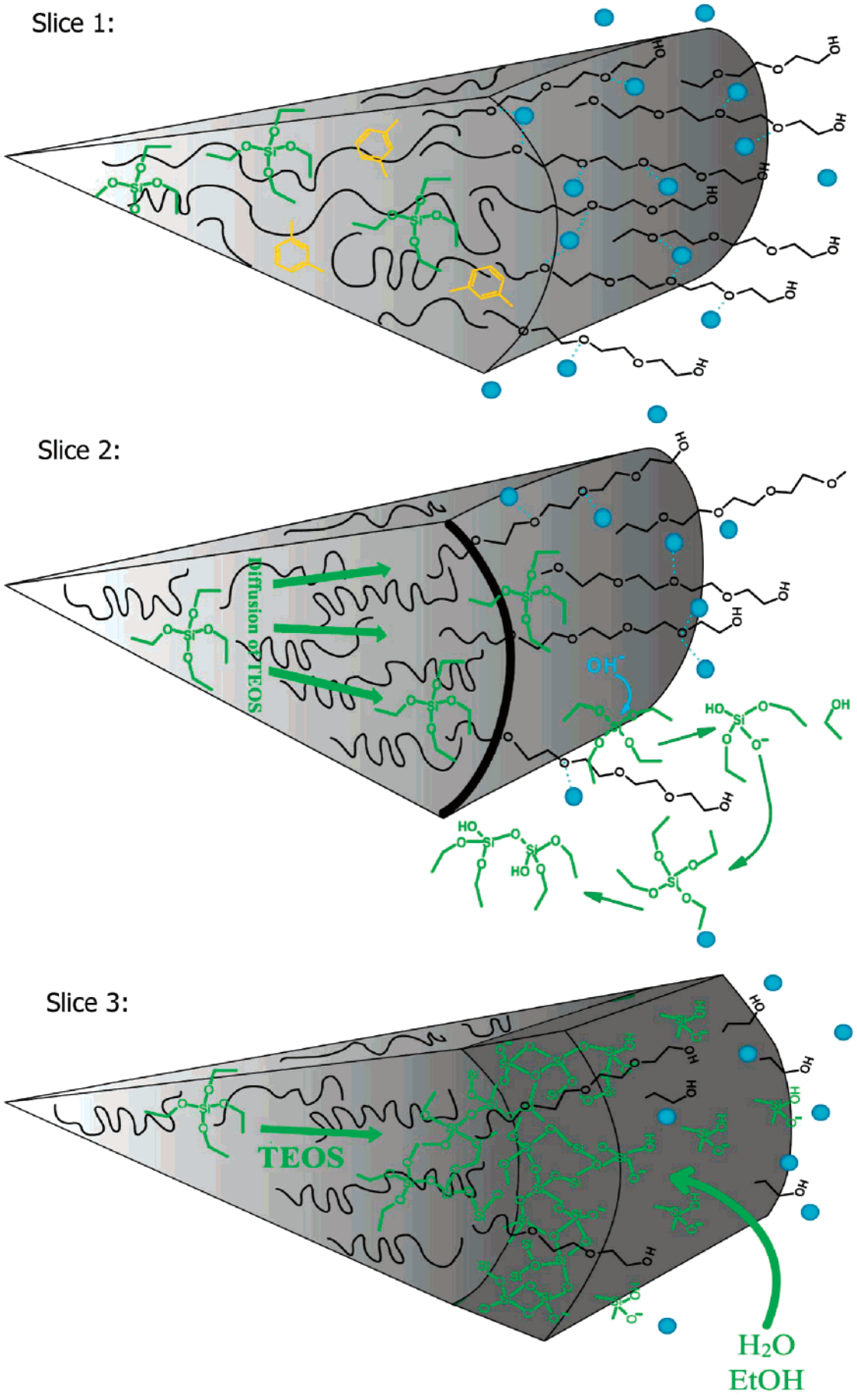

dissolves-like"); compounding of mixtures of PE@silica and polyolefin also was tested successfully in our laboratories.

Acknowledgment. Supported by the Nano Functional Materials (NFM) MAGNET Program of the Israel Ministry of Trade and Industry, the Infrastructure (Tashtiot) Program of the Israel Ministry of Science, and the European Functionalized Advanced Materials and Engineering Hybrids and Ceramic (FAME) Network of Excellence (NOE). We thank Guillaume Laurent for technical assistance with the NMR experiments.

JA0653167